Corrosion of Aluminum, Copper, Brass and Stainless Steel 304 in Tequila

Alejandra Carreon-Alvarez[1], Rocío Castañeda Valderrama[1], Jorge Avalos Martínez[2],
Arturo Estrada-Vargas[3], Sergio Gómez-Salazar[3], Maximiliano Barcena-Soto[4], Norberto Casillas[4,*]

[1] Departamento de Ciencias Exactas y Naturales, Universidad de Guadalajara-Centro Universitario de los Valles, Carretera Guadalajara-Ameca km. 45.5, Ameca, Jalisco, México, 46600
[2] Departamento de Química, Área de Electroquímica, Universidad Autónoma Metropolitana-Iztapalapa, Av. San Rafael Atlixco # 186, Col. Vicentina, Del Iztapalapa México D.F, 09340.
[3] Departamento de Ingeniería Química, Universidad de Guadalajara-Centro Universitario de Ciencias Exactas e Ingenierías. Blvd. Marcelino García Barragán #1451, Guadalajara, Jalisco, México 44430.
[4] Departamento de Química, Universidad de Guadalajara-Centro Universitario de Ciencias Exactas e Ingenierías. Blvd. Marcelino García Barragán #1451, Guadalajara, Jalisco, México 44430.
[*]E-mail: ncasa@hotmail.com

In this study corrosion rates of aluminum, copper, brass and Stainless Steel 304 (SS 304) in tequila are reported from potentiodynamic polarization and Electrochemical Impedance Spectroscopy (EIS) measurements. A simple kinetic model is proposed to analyze the polarization data and to establish a comparison with EIS measurements. For the examined metals/alloys, aluminum exhibited the highest corrosion rate of ca. 6.1 pm s^{-1} with a pitting corrosion tendency after being exposed to tequila (pH = 3.6). SS 304 was the most stable metal with a corrosion rate of 0.28 pm s^{-1}. The corrosion rate trends for all the investigated metals/alloys from potentiodynamic polarization and EIS measurements are Al > Cu > brass > SS 304.

1. INTRODUCTION

Without any doubts the most popular contemporary alcoholic beverage in Mexico is tequila, which is made from the juice of cultivated variants of *Agave Azul Tequilana Weber* [1]. At some stage of the tequila production, either raw materials or finished product are in contact with equipment made of different metals susceptible to suffer corrosion. For instance, at the early stage of tequila production, agave is cooked in stainless steel (SS) autoclaves or in brick ovens with a carbon steel

door. In a subsequent stage of the process, cooked agave is milled to extract fermentable juices, so it becomes in contact with SS or carbon steel roller mills again. Once in the yeast fermentation processes, the extracted agave juice is stored in SS tanks. SS or copper pot stills are used during distillation to obtain *ordinario* (product of the first distillation in tequila production) or *tequila* (product of the second distillation). This practice induces the incorporation of metals into these alcoholic beverages, such as copper, whose dissolution is promoted by an acidic pH (ranging from 3.5 to 4.9), high temperature and the presence of oxygen, chloride or organic compounds [2-5]. In addition, to the above mentioned metal incorporation routes, there are other sources of metals that may find the way into tequila coming from the water supplied to the process as well as metals contained in raw materials [1].

Only few reports in the literature deal with corrosion rate of metals in contact with spirituous beverages, such as tequila. Some of them are mostly related to specific corrosion studies for either pure ethanol or its mixtures due to its potential applications as a fuel in internal combustion engines [6]. More recently a corrosion study was reported for aluminum-bronze dental alloys used as dental implants in contact with different beverages (alcoholic drink, natural and artificial fruit juices, vinegar, soft drinks and milk) [7]. Corrosion results from this study suggested that the most aggressive one was the artificial orange juice, which produced a corrosion rate one order of magnitude higher than saliva [7]. In a previous work by our research group, the corrosion rate of copper in tequila was determined at different temperatures using the weight loss method [3]. The results from this study demonstrated that copper builds up in tequila during the distillation process when it is carried out in copper pot stills, and a corrosion rate for copper of about 3.22 pm s^{-1} at 65 °C was determined. At higher temperatures the copper corrosion rate decreased due to the depletion of diluted oxygen concentration in tequila. Other studies conducted by our research group have been aimed to develop electrochemical methods to analyze copper in tequila or conducting more systematic studies of the incorporation of metals into tequila [8-10].

Nowadays, more strict regulations have been imposed concerning the maximum concentration of metals allowed in tequila by the appellation of origin by European Community and Mexico as a result of the mutual recognition and protection of designations for spirituous drinks (CRT 1997) [11]. In order to comply with these regulations, tequila producers are selecting different construction materials for their process equipment. As a consequence, copper pots still are being replaced by stainless steel (SS) pot stills [11, 12]. Nevertheless some sections of the SS pot still are still made of copper, such as the heating coil or the goose neck of the distillation column. These copper sections are used because of the catalytic properties of copper to remove and/or transform bad odors caused by volatile sulfur-containing compounds produced during fermentation, but they can constitute another source of copper into tequila [13-15]. Despite the fact that raw material and tequila are neither in contact with aluminum nor brass equipment sections along the production line, tequila can be stored in vessels made of these materials so there is some interest for investigating them.

The aim of this work is to obtain reliable corrosion rates of aluminum, copper, brass and stainless steel 304 in tequila at room temperature. To pursue this objective, corrosion rate measurements were performed using two electrochemical techniques: 1) Potentiodynamic Polarization, whereby corrosion current density, corrosion potential, Tafel parameters (e.g., anodic and cathodic

slopes), charge transference resistance and corrosion rate experimental data were further analyzed by a proposed simple kinetic corrosion model; and 2) Electrochemical Impedance Spectroscopy (EIS), whereby experimental data were analyzed with an equivalent circuit method.

2. EXPERIMENTAL

2.1 Electrodes preparation

Aluminum, copper, SS 304 and brass samples of 1 inch length were cut from ¼ inch diameter rods and embedded in Teflon to prepare metal disk electrodes. These exposed metal surfaces were polished with emery paper (600-1200 grit) and suspended in a mechanical polisher (Micro Star 2000) with alumina powder (0.05 μm) to obtain a mirror-type finishing. The metal electrodes were thoroughly rinsed with bi-distilled water and immersed in isopropyl alcohol (Golden Bell, USA). A final washing was carried out with acetone for 5 minutes to eliminate organic residues and the remaining alumina. For all metals/alloys, the electrodes were air dried and placed into an electrochemical cell with an exposed area of ~ 0.19 cm^2 in order to obtain the potentiodynamic polarization curves and to apply EIS.

2.2 Potentiodynamic polarization curves (PR)

A typical three-electrode electrochemical corrosion cell was used in all the experiments. A saturated calomel electrode (SCE) was used as reference. All measured potentials were referred to this electrode. A platinum foil was used as the counter electrode. The Aluminum, copper, brass and SS 304 samples were used as working electrodes. All experiments were carried out using ordinario without supporting electrolyte nor deareation. A potentiostat (Solartron Analytical model SI1287), controlled by a personal computer, equipped with a GPIB card and the commercial software CorrWare® was employed to obtain the potentiodynamic polarization curves. Before each experiment, the open circuit potential (OCP) was recorded for at least 30 min. Polarization curves were obtained potentiodinamically; the linear potential sweep was performed at a ±250 mV potential window around the measured OCP, from the cathodic to the anodic side, at scan rates of 0.1 and 1 mV s^{-1}.

2.3 Electrochemical Impedance Spectroscopy (EIS)

All impedance measurements were performed at the same three-electrode cell arrangement than potentiodynamic polarization curves. The potentiostat/galvanostat (Solarton 1287) was coupled to a frequency response analyzer (FRA) (Solartron 1260). The instruments control and the data acquisition were done by the personal computer by means of the commercial software Zplot®. In order to establish a pseudo-steady state, each sample was held at least for 30 minutes at OCP previous to the EIS experiments. The fixed potentials at which EIS measurements were performed were respectively: -0.13, -0.50, -0.10 and -0.08 V vs. SCE for SS 304, Al, Cu and brass. An alternating voltage with

amplitude of 10 mV, at frequencies in the range of 10 KHz to 10 mHz, 10 points per decade, was imposed. The experimental data were tested to satisfy the postulates of the fundamental impedance theory by using the Kramers-Kroning transformation [16]. The impedance spectra were fitted to an equivalent circuit by means of the commercial software Boukamp®.

2.4. Conductivity and pH measurements

Conductivity and pH measurements were performed using a pH/conductivity Orion 4 Star® Benchtop, equipped with an Orion 011510MD conductivity cell.

2.5. Solution

Ordinario was produced in the Centro de Investigación y Asistencia en Tecnología y Diseño del Estado de Jalisco (CIATEJ) and used as received. Ordinario and tequila are respectively the products of the first and second distillation in the tequila production. The major difference between these two beverages is the ethanol content of 25-30% w/w for the first one and 38-42% w/w for the second one, but the organic matrix remains almost the same [17-18].

3. RESULTS AND DISCUSSION

3.1 Potentiodynamic polarization curves

Ordinario has an acidic average pH of 3.61 and a low conductivity of 101 μS cm^{-1}. Under these circumstances polarization curves may require a correction with the solution resistance [19]. However, in our case, we substantially reduced the R_s solution value by placing the reference and counter electrodes as near as possible to the working electrode and maintaining the same three-electrode cell configuration for performing both potentiodynamic polarization curves and EIS experiments. This strategy was indeed effective for minimizing the R_s contribution to the potential drop which avoids further corrections. Thus, it is possible to establish a direct comparison between the experimental results obtained by potentiodynamic polarization and EIS techniques as shown below.

Figure 1 shows a set of potential, E, vs. logarithm plots of the absolute value of the current density, i, for aluminum, SS 304, brass and copper in ordinario from polarization resistance measurements at 0.1 mV s^{-1}. Cu and brass display a rapid current density increase with potential in the anodic branch, indicating the presence of a less protective oxide film in ordinario. On the contrary, SS 304 follows a nonlinear trend at high anodic overpotentials, due to the formation of a passive surface. Differently to previous metals, aluminum denotes a sudden increase of the current density at ca. -0.4 V vs. SCE, attributed to the formation of a less protective oxide layer and a tendency to breakdown the oxide film and to develop pitting corrosion [19]. The cathodic branches for SS 304 and brass display a linear trend at high cathodic overpotentials. Cu and Al show deviations from single-specie cathodic reactions. It is worth noting that ordinario is a rather complex mixture of more than 125 constituents

and some of them may also contribute to the corrosion of the investigated metals even at low concentrations, for example, acetic acid or even the presence of chloride ions [17-18].
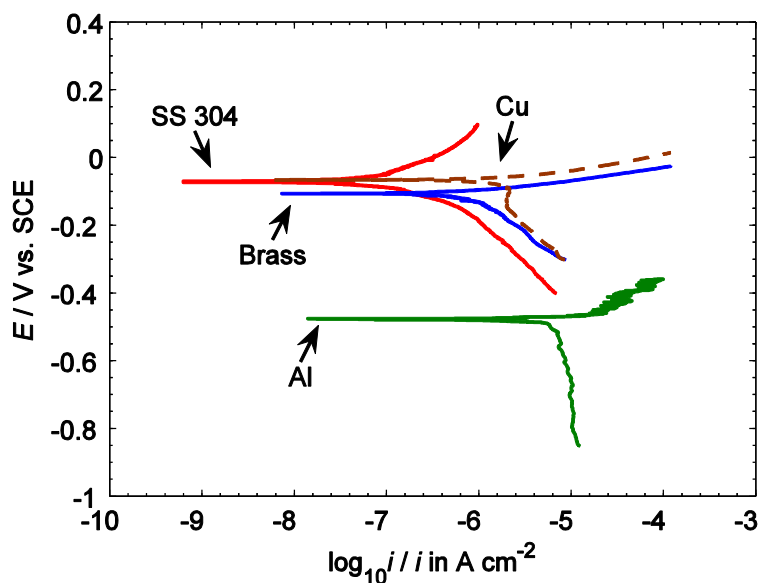
Figure 1. Tafel plots of aluminum, copper, brass and SS 304 in ordinario at a scan rate of 0.1 mV s^{-1}.

From the potentiodynamic polarization data we can readily obtain kinetic and thermodynamic information by following standard procedures, such as the anodic (β_a) and cathodic (β_c) Tafel slopes, the corrosion potential (E_{corr}), polarization resistance, R_p and the corrosion current density (i_{corr}). The polarization resistance is defined as the slope of the potential-current density plot evaluated at E_{corr} [19].

$$Rp = \frac{dE}{di}\bigg|_{Ecorr} \tag{1}$$

Thus, the Stern-Geary equation is used to obtain i_{corr},[19, 20], whereas the corrosion rate, v, is calculated from equation (3) [19]:

$$i_{corr} = \frac{\beta_a \beta_c}{2.303(\beta_a + \beta_c)} \cdot \frac{1}{R_p} = \frac{B}{R_p} \tag{2}$$

$$v = \frac{10^{10} \cdot i_{corr} \cdot EW}{F \cdot d} \tag{3}$$

where all the variables have their usual meanings, v has units of pm s^{-1}, i_{corr} is in A cm^{-2}, EW is the equivalent weight of the metal/alloy (g eq^{-1}), F is the Faraday constant (96500 C eq^{-1}), d is the density of the metal/alloy (g cm^{-3}) and 10^{10} is a conversion factor [19]. For the case of metals where the

anodic or cathodic Tafel slope could not be calculated, an extrapolation of the calculated Tafel line to E_{corr} is used as strategy for calculating i_{corr} instead of using equation (2).

Table 1 summarizes kinetic data calculated from Tafel plots appearing in Figure 1. The corrosion potential, E_{corr}, is almost the same for SS 304 and copper, slightly lower than brass, and it has a much less noble value for aluminum. Corrosion rates for all metals/alloys follow the order: Al > Cu > Brass > SS 304. The lowest corrosion rate was observed for SS 304 (0.28 pm s^{-1}), which is slightly lower than brass (0.30 pm s^{-1}), and they can be considered equal for practical purposes. Interestingly, brass has a better corrosion resistance than copper in ordinario. Valcarce et al. have reported corrosion rates of copper and brass in contact with tap water [21]. Their results showed that brass corrodes at slower rate than copper in tap water, due to the presence of zinc as an alloy element. They reported values of i_{corr} for copper and brass of 0.35 and 0.20 µA cm^{-2} respectively. However, higher i_{corr} values in ordinario can be expected, since it is a more acidic, aerated and resistive media, which may promote a higher corrosion rate.

Table 1. Electrochemical parameters at pseudo-steady state conditions obtained by the polarization resistance method.

Metal	E_{corr} / V vs. SSE	β_a / V	β_c / V	R_p / Ω cm^2	i_{corr} / µA cm^{-2}	v / pm s^{-1}
SS 304	-0.07	-	0.26	219 800	0.39	0.28
Al	-0.47	-	0.83	1 250	5.9	6.1
Brass	-0.10	0.04	0.19	14 700	0.41	0.30
Cu	-0.06	0.04	-	5 720	2.2	1.6

According to the above mentioned findings the most suitable material to be used in tequila processing is SS 304, which has a passive state with the lowest corrosion rate of 0.28 pm s^{-1}.

Although it is possible to extract the kinetic parameters from the polarization curves it is worth noting that there are some experimental difficulties that should be addressed and be taken into consideration. Firstly, the presence of non-faradic currents which are due to the charge/discharge of capacitive layers may contribute to the measured current. For instances, at potentials near E_{corr}, the anodic and cathodic currents are small enough and can be affected by non-faradic contributions. Therefore, data analysis provides inaccurate values for E_{corr} and consequently for R_p and i_{corr}. Since the values of these non-faradic currents increase with the potential sweep rate, there is a maximum acceptable value for a given experiment, which may extend with the elapsed experiment time. On the other hand, polarization data from corrosion measurements are often time-dependent for long-time experiments and they may not return reliable data for a pseudo-stationary state of the system. Thus, the only alternative to perform a short-time polarization resistance measurement at slow potential scan rate is by reducing the potential sweep window. According to the above mentioned limitations, a non-mass-transfer model considering non-faradic currents was proposed to calculate all thermodynamic and kinetic parameters, including i_{corr}, without the linear E vs. log$|i|$ behavior at high overpotentials from the polarization resistance data [16].

Here, the total current results from adding the anodic current from the metal oxidation, the cathodic current from the reduction reaction and the capacitive current from the charging/discharging processes:

$$i = i_a + i_c + i_{nf} \tag{4}$$

where anodic and cathodic currents are described by Equations (5) and (6).

$$i_a = K_a \exp(b_a E) \tag{5}$$

$$i_c = K_c \exp(b_c E) \tag{6}$$

In equations (5) and (6), K_a, K_c, b_a and b_c are constants which include kinetic parameters for the non-mass-transfer model for both the oxidizing and reducing species. The influence of the double layer capacitance charging is taken into account by equation (7) [16]:

$$i_{nf} = C \frac{dE}{dt} \tag{7}$$

where *dE/dt* is the scan rate used in the potentiodynamic polarization experiment. The values for K_a, K_c, b_a, b_c and C are adjusted by fitting the current-potential data of Fig. 1 near the E_{corr} (± 0.05 V) value from Table 1, by means of the Levenberg-Marquardt method, implemented in a program written with the commercial software MatLab$^{®}$.

E_{corr} is considered as a potential at which $i_a = i_c = i_{corr}$. At this potential, R_p is obtained from equation (7):

$$R_p^{-1} = R_a^{-1} + R_c^{-1} \tag{7}$$

where R_a and R_c are the reciprocal of the partial derivations $\partial i_a / \partial E$ and $\partial i_c / \partial E$ evaluated at E_{corr}:

$$R_{p,a} = \lfloor b_a K_a exp(b_a E_{corr}) \rfloor^{-1} \tag{8}$$

$$R_{p,c} = \lfloor b_c K_c exp(b_c E_{corr}) \rfloor^{-1} \tag{9}$$

Thus, equations (8) and (9) allow the calculation of the polarization resistances for both the oxidizing and reducing agents for the corrosion reaction. However, only the overall polarization resistance, R_p, can be used for comparison with other techniques such as the classic polarization resistance method and EIS.

Table 2 summarizes the kinetic and thermodynamic data obtained from the above mentioned model. An acceptable data fitting for aluminum was not possible due to its noisy current behavior at

low overpotentials, so a polarization sweep at a scan rate of 1 mV s^{-1} was performed for this particular metal. Since the proposed kinetic model takes into account the non-capacitive currents rise due to a higher scan rate, results are not expected to be very different to the ones obtained at 0.1 mV s^{-1}. For all metals/alloys, E_{corr} values coincide better with the OCP values obtained from EIS experiments, than the ones obtained from the plain polarization resistance method. The R_p values follow the same order to the ones obtained from the polarization resistance analysis, which is, SS 304 > brass > Cu > Al. The corrosion rate values also follow the same trend, but the values of v for SS and brass are different.

Table 2. Electrochemical parameters at pseudo-steady state conditions obtained by the polarization resistance method.

Metal	E_{corr} / V vs. SCE	Rp / Ω cm^2	i_{corr} / μA cm^{-2}	v / pm s^{-1}	Cdl / F cm^{-2}
SS	-0.13	159 700	0.03	0.01	2.02×10^{-3}
Al*	-0.46	10 900	9.86	2.13	7.30×10^{-3}
Brass	-0.11	17 726	0.74	0.27	1.68×10^{-3}
Cu	-0.08	13 100	1.37	0.47	1.88×10^{-3}

*Al data obtained at 1 mV s^{-1}.

3.2 EIS analysis

Fig. 2a shows Nyquist plots for aluminum, copper, brass and SS 304 in ordinario at pseudo-steady state conditions. Marks in the figure correspond to experimental data and solid lines to theoretical predictions, which are further explained later.
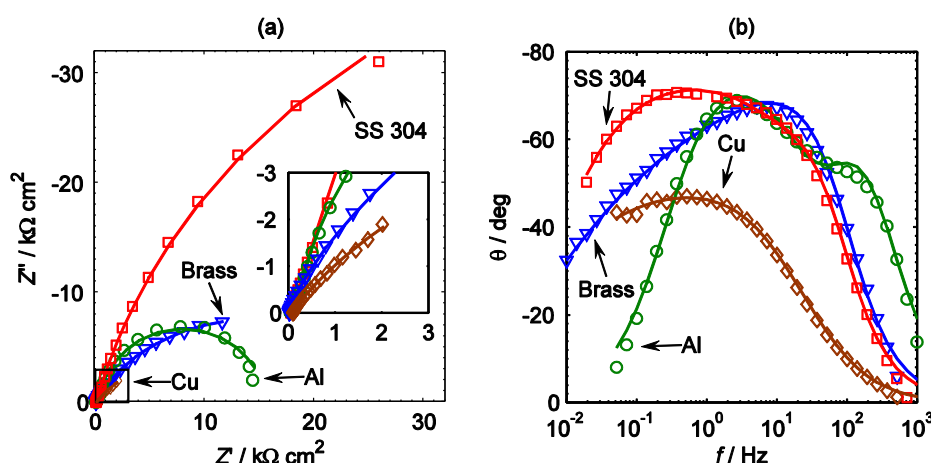

Figure 2. (a) Nyquist and (b) Bode phase diagrams of aluminum, copper, brass and stainless steel in ordinario without stirring. All measurement were performed at open circuit potential, with a 10 mV amplitude and a 10 kHz – 0.01 Hz frequency sweep, employing a two-electrode configuration.

The inset in Fig. 2a is a close-up of Cu data. Nyquist's plots for Cu, brass and SS 304 display incomplete semicircles, denoting metals with protective oxide films [22]. For the case of aluminum, the presence of a semicircle is attributed to the formation of an interfacial oxide layer, where Al is oxidized to Al^+ intermediates and later on oxidized to Al^{3+} at the oxide solution interface where O^{2-} or OH^- can also be formed [23]. Brass and copper data show more depressed semicircles that can be attributed to the lack of uniformity of the current distribution. This behaviour can be also related to the presence of a less uniform oxide film, which somehow induces differences in the local impedance and a time constants distribution along the electrode surface. Figure 2b shows Bode phase diagrams of the EIS data for the four metals/alloys investigated, where two average time constants become readily evident for all them.

Fig. 3 shows a proposed equivalent circuit to further investigate the properties of the metals/alloys-ordinario interface to explain the experimental data. The equivalent circuit includes a solution resistance, R_s, oxide layer capacitance, C_{ox}, and resistance, R_{ox}, a constant phase element, CPE_{dl}, for the double-layer capacitance and the polarization resistance, R_p. This model has been used previously by Valcarce et al., who considered that the corroding electrodes may have various types of heterogeneities that can be better taken into account by using a constant phase element (CPEs) instead of a simple capacitor [21].
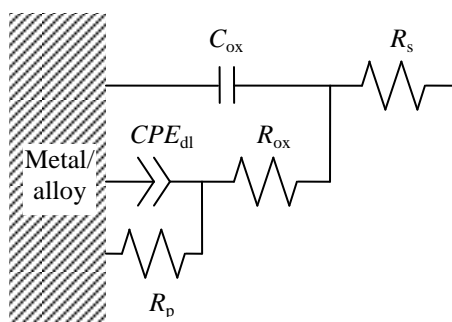
Figure 3. Equivalent circuits used to fit EIS data for copper, brass, aluminum and SS 304 in ordinario.

EIS data were fitted to the equivalent circuit elements for all metals/alloys by means of the commercial software Boukamp®. The theoretical curves are drawn as solid lines in Fig. 2. Fitting values are shown in Table 3, where the estimated double-layer capacitance, C_{dl}, was calculated with the formula:

$$C_{dl} = CPE_{dl}(\omega_{max})^{n_{dl}-1} \tag{10}$$

where ω_{max} is the characteristic frequency at which the imaginary part of the impedance, Z'', reaches its maximum [20]. For metals/alloys where the experimental data do not show a maximum Z'' value, extrapolations of the theoretical data to lower frequency values were performed.

Table 3. Parameters obtained by fitting EIS data to the equivalent circuit using the Boukamp code for SS 304, aluminum, copper and brass in ordinario.

Metal	R_s / Ω cm^2	C_{ox} / F cm^{-2}	R_{ox} / Ω cm^2	C_{dl} / F cm^{-2}	n_{dl}	R_p / Ω cm^2
SS 304	58	3.87×10^{-5}	440	2.79×10^{-4}	0.75	112 100
Al	44	1.02×10^{-5}	350	2.57×10^{-5}	0.88	15 400
Brass	24	7.22×10^{-5}	178	1.01×10^{-3}	0.57	29 900
Cu	102	6.62×10^{-5}	23	3.65×10^{-3}	0.55	15 000

It was possible for all the investigated metals/alloys to represent the oxide charging/discharging process as a pure capacitance. However, the double-layer formation at the electrolyte-solution interface showed a time constants distribution and had to be represented by a CPE. This distribution is less dispersed for Al and SS 304, which n_{dl} values are respectively 0.75 and 0.88, and more dispersed for Cu and brass. Since C_{dl} and C_{ox} are parallel in the equivalent circuit proposed, the sum of these two values can be compared to the total capacitance value, C, obtained from the potentiodynamic polarization data and presented in Table 2. The total capacitances from both methods are similar for Cu and brass, but not for SS 304 and Al. Likely these differences could imply the requirement of improving the formula for i_{nf} in the proposed kinetic model.

The sum of R_s and R_{ox} is less than 3% of the R_p value for all metals/alloys. This result somehow validates the fact of not making corrections to the data from polarization resistance measurements with the R_s values obtained from EIS data. The R_p values, which relate inversely to the corrosion rate, follow the order: SS 304 > brass > Al > Cu. These values show a little variation with respect to the R_p values in Tables 1 and 2, obtained by the polarization resistance method. However, from both PR and EIS methods it can be concluded that SS 304 has the highest R_p value, with at least one order of magnitude greater than any other metals, whereas Al has the lowest R_p values and hence a higher corrosion rate. Therefore, corrosion rate results obtained from both potentiodynamic polarization and EIS methods confirm that SS 304 is the most suitable material to be used in tequila processing.

4. CONCLUSIONS

Corrosion rate measurements for the metals/alloys investigated follow the order Al > Cu > brass > SS 304 obtained by potentiodynamic polarization curves and EIS analysis. A classical polarization resistance method and a rather simple kinetic model without any mass transport considerations were used to analyze potentiodynamic polarization data, providing coherent results. An equivalent electric circuit was proposed to analyze EIS experimental data. Stainless Steel 304 presented the lowest corrosion rate, a result which coincides with both used methods.

References

1. J. G. Ibanez, A. Carreon-Alvarez, M. Barcena-Soto, N. Casillas, *J. Food Compos. Anal*., 21 (2008) 672
2. A.Moutsatsou, E. Chalarakis and G. Zarangas, *J. Hazard. Mater*., 96 (2003) 53
3. A.Carreon, N. Casillas, V. González-Álvarez, R. Prado-Ramírez, *Mater. Performance* 40 (2001) 50
4. M. Cedeño, Crit. Rev. Biotechnol., 15 (1995) 1
5. R. Prado-Ramírez, V. González-Alvarez, C. Pelayo-Ortiz, N. Casillas, M. Estarrón and H. E. Gómez-Hernández, *J. Food Sci. Technol*., 40 (2005) 701
6. J. P. Souza, O. R. Mattos, L. Sathler and H. Takenouti, *Corros. Sci.*, 27 (1987) 1351
7. G. S. Duffó and S. B. Farina, *Chem. Phys*., 115 (2009) 235
8. A.Carreon-Alvarez, N. Casillas, J. G. Ibanez, S. Gomez-Salazar, F. Hernandez, R. Prado-Ramírez and M. Barcena-Soto, *Anal. Lett*., 41 (2008) 469
9. C. Rodríguez Flores, J. A. Landero Figueroa, K. Wrobel and K. Wrobel, *Eur. Food Res. Technol*., 228 (2009) 951
10. S. G. Ceballos-Magaña, J. M. Jurado, M. J. Martín and F. Pablos, *J. Agric Food Chem*., 57 (2009) 1372
11. Diario Oficial de la Federación, Mexico D. F., L152 (11/07/1997) 16.
12. A.S. Fouda, H. A. Mostafa, H. M. El-Abbasy, *J. Appl. Electrochem*., 40 (2010) 163
13. D. Reaich, Proc. 5th. Aviemore Conf. Malt. Brew. Dist. Aviemore, Inverness, UK, May 25-28, (1998) 141.
14. M. Cedeño Cruz, Tequila Production from agave: historical influences and contemporary process, in: The Alcohol textbook, Ed. by K. A. Jacques, Nottingham University Press, Nottinghamshire (2003)
15. A.Valenzuela-Zapata and G. P. Nabhan, ¡Tequila!, University of Arizona Press, Arizona (2003)
16. M. E. Orazem and B. Tribollet, Electrochemical Impedance Spectroscopy, Wiley, New Jersey (2008)
17. S. M. Benn and T. L. Peppard, *J. Agric. Food Chem*., 44 (1996) 557
18. A.Carreon-Alvarez. Estudio electroquímico de la remoción de cobre en tequila. Universidad de Guadalajara, Jalisco (2003)
19. D. A. Jones, Principles and Prevention of Corrosion, 2nd ed., Prentice-Hall, New Jersey (1996)
20. M. Stern and A. L. Geary, *J. Electrochem. Soc*. 104 (1957) 56
21. M. B. Valcarce, S. R. De Sánchez and M. Vázquez, *J. Matter. Sci*., 41 (2006) 1999
22. R. Cottis and S. Turgoose, Electrochemical Impedance and Noise, NACE International, Texas (1999)
23. H. J. W. Lenderink, M. V. D. Linden and J. H. W. De Wit, *Electrochim. Acta*, 38 (1993) 1989